ELSEVIER

Nuclear Instruments and Methods in Physics Research A 411 (1998) 351–364

NUCLEAR INSTRUMENTS & METHODS IN PHYSICS RESEARCH Section A

Response of NaI(Tl) to X-rays and electrons

Leonard R. Wayne[a,*], William A. Heindl[a], Paul L. Hink[b], Richard E. Rothschild[a]

[a] *Center for Astrophysics and Space Sciences, University of California, San Diego, La Jolla, CA 92093-0424, USA*
[b] *Department of Physics, Washington University, St. Louis, MO 63130-4899, USA*

Received 31 October 1997

Abstract

Measurements of the light output response of NaI(Tl) to X-rays were taken as part of the pre-flight calibrations of the High Energy X-ray Timing Experiment (HEXTE), currently in orbit aboard NASA's Rossi X-ray Timing Explorer. These measurements cover the energy range 12–159 keV. Radionuclides and fluorescent sources were used to provide a coarse sampling of this energy range, and a tunable X-ray monochromator was used to provide a fine scale mapping around the iodine K-edge (33.17 keV), where the light output response of NaI(Tl) varies rapidly with energy. The light output response to X-rays is measured to an accuracy of $\pm$ 0.7%.

In addition to presenting the results of these X-ray calibrations, we use these data to infer the response of NaI(Tl) to electrons in the energy range 0.1–125 keV. This is done using the procedure of Collinson and Hill [Proc. Phys. Soc. 81 (1963) 883], modified to take into account systematic effects that have been noted in the literature and to improve the model that is used to describe the cascade liberation of electrons that follows the absorption of an X-ray in the crystal. The Collinson and Hill procedure is particularly well suited to work with X-ray data, such as ours, that include detail at energies just above the iodine K-edge; the data here are used to determine the response of NaI(Tl) to low energy electrons, a point of contention in the literature. Our measurements of the electron response extend down to lower energies than have been examined in the past. The light output response to electrons is measured to an accuracy of $\pm$ 90% at 0.1 keV, $\pm$ 50% at 1 keV, $\pm$ 5% at 10 keV, and $\pm$ 4% at 100 keV.

Keywords: NaI(Tl): X-ray response; Electron response; Scintillation response; Surface effects

1. Introduction

The High Energy X-ray Timing Experiment (HEXTE) [1] is currently in orbit aboard NASA's Rossi X-ray Timing Explorer. HEXTE employs NaI(Tl) scintillation crystals to detect X-rays in the energy range 15–250 keV. It is designed to observe spectra and temporal variability from galactic and extragalactic sources, such as neutron stars, black holes, white dwarfs, and active galactic nuclei.

As part of the pre-flight calibration of HEXTE, measurements were made of the light output response of the NaI(Tl) crystals to X-rays. These measurements were done to assist in the development of the "instrument response matrix", which is used in determining the spectral characteristics of

* Corresponding author. Tel.: + 1 619 822 1260; fax: + 1 619 534 2294; e-mail: lwayne@ucsd.edu.

0168-9002/98/$19.00
PII: S0168-9002(98)00193-4

data taken on orbit. The calibration measurements were made both with a tunable X-ray monochromator at the Brookhaven National Synchrotron Light Source, as well as with laboratory radionuclides and fluorescent sources. The measurements cover the energy range 12–159 keV.

In addition to presenting results from these X-ray calibrations, we report on the use of these X-ray data to infer the response of NaI(Tl) to electrons. The electron response is determined using the procedure of Collinson and Hill [2].

Briefly, the Collinson and Hill procedure can be summarized as follows. The light output response of NaI(Tl) to X-rays is conceptually recast in terms of the light output response of NaI(Tl) to electrons. A model is created of the distribution of electrons that are liberated as an incident X-ray loses its energy to the NaI(Tl) crystal. The strategy is to look at pairs of X-ray energies that lead to "mostly" similar distributions of liberated electrons. By subtracting the light output measurement of one member of a pair from the other, the "mostly" similar parts of the two electron distributions cancel out, and what is left can often be interpreted as arising primarily from a single electron of known energy. In this way, one infers a curve to describe the response of NaI(Tl) to single electrons as a function of energy.

A number of authors have estimated the response of NaI(Tl) to electrons (see, e.g., Refs. [3–11]) using various techniques. At energies above ~ 30 keV these estimates are in generally good agreement, with a spread of no more than 4%. However, at energies below 30 keV there is significant variance in the reported results.

In our derivation of the electron response curve we account for several systematic effects that can distort the low energy results obtained from the Collinson and Hill procedure. First, we extend the procedure to include a more detailed model of the production of Auger electrons and photoelectrons following X-ray absorption in the crystal. Second, our X-ray measurements include a detailed mapping of the response of NaI(Tl) in the energy region just above the iodine K-edge (33.17 keV); it is especially useful to have X-ray response data here when using the Collinson and Hill procedure. Third, we include the K-escape corrections to the Collinson and Hill method noted by Meggitt [7]. Fourth, we omit from the Collinson and Hill procedure a step that we believe actually hurts the results more than it helps. Fifth, we perform a careful examination to ensure that our data show no sign of being distorted by surface effects.

2. Experimental setup

2.1. The HEXTE phoswich detectors

HEXTE consists of eight identical NaI(Tl)/CsI(Na) phoswich detectors. Each detector (Fig. 1) employs a circular NaI(Tl) primary crystal which is one eighth of an inch thick and has a face area of 40.7 in^2 (263 cm^2). The amount of Tl doping is roughly 1.3×10^{-3} mol Tl/mol NaI. This crystal is optically coupled to a 2.238 inch thick CsI(Na) crystal which is used for anti-coincidence rejection of partial energy loss events in the NaI(Tl). Pulse shape discrimination is used to distinguish whether energy absorption occurred in the NaI(Tl) or the CsI(Na) or both. If any energy loss occurs in the CsI(Na), then the event is rejected. The CsI(Na) crystal is coupled to a fused quartz window in the rear of the hermetically sealed crystal housing. A ruggedized Hamamatsu R877 five inch photomultiplier tube with a spectral response range of 300–650 nm is optically coupled to the outside of the quartz window. Thus the scintillation light produced by the NaI(Tl) crystal passes though the CsI(Na) crystal and quartz window before reaching the photomultiplier tube. The front of the NaI(Tl) crystal and the sides of both the NaI(Tl) and

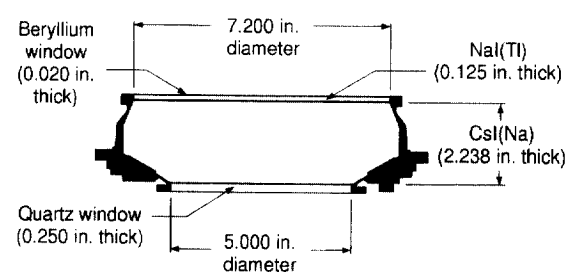

Fig. 1. Cutaway view of crystal assembly on one of eight HEXTE NaI(Tl)/CsI(Na) phoswich detectors.

CsI(Na) crystals are covered with teflon for diffuse reflection of the scintillation light. The crystal surfaces are highly polished to optimize light collection and therefore improve the detector's pulse height resolution.

2.2. Brookhaven National Synchrotron Light Source

The X-ray response measurements include the use of a tunable X-ray monochromator on Beamline X27A at the National Synchrotron Light Source at Brookhaven National Laboratory. This beamline station receives 10–60 keV X-rays generated by electrons circulating in the main storage ring. A tunable double Bragg reflection monochromator was used to select the energies of interest. The energy resolution for this monochromator is on the order of 10 eV. The monochromator calibration was checked frequently by measuring K-shell photoelectric absorption edge energies of various elements placed in the output beam of the monochromator. In this way the monochromator energy calibration was kept to within $\pm 0.2\%$.

The very high intensity of the synchrotron beam was reduced to acceptable levels for the detector and its support electronics by blocking all but a tiny portion of the monochromatic X-rays exiting the monochromator. The spot size at the detector was less than 1 mm^2 and was located at the center of the crystal. The remainder of the phoswich was shielded by lead bricks. When necessary, the beam intensity was further attenuated by the introduction of metallic foils into the beam. All measurements were made with counting rates of less than 1250 counts per second in order to avoid electronic pulse pileup.

The electronics setup is shown in Fig. 2. A test pulse generator was used to monitor the gain of the analog electronics and the zero offset of the pulse height analyzer. The time constant for the linear shaping amplifier was set to 500 ns, and the bi-polar output was used. The measurements were done with a flight spare detector and standard NIM series laboratory electronics (not the flight electronics boards).

The monochromator was stepped in energy increments of 1–2 keV over most of the allowed 10–60 keV energy range. The step size was reduced

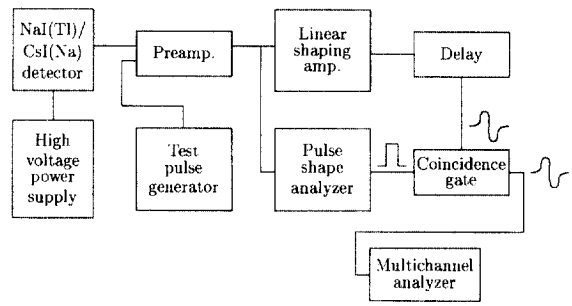

Fig. 2. Electronics setup used to measure the light output response of NaI(Tl) to X-rays.

to as little as 0.05 keV in the energy region around the iodine K-edge (33.17 keV). This energy region was mapped in such fine detail since the X-ray response of NaI(Tl) varies rapidly there. In addition, it is an energy region of particularly important astrophysical interest (e.g., cyclotron absorption features have been detected near 30 keV).

Corrections are applied to the data to account for offsets in the pulse height measurement. We define offset according to

$$PH = gain \cdot L + offset, \tag{1}$$

where PH is the measured pulse height, and L is the amount of light output from the crystal. Correcting for offset is necessary because a non-zero offset would distort the proportional relationship we desire between the light output and the recorded pulse height. Offset is measured by the use of a test pulse generator (see Fig. 2) with various pulse height attenuation settings.

Fig. 3 shows an example of a small systematic effect that appears in our monochromator data. A slight asymmetry is detected in the spectra of many of the peaks we recorded. Spectral fits with a single Gaussian give poor residuals. The residuals are substantially improved by the addition of a second Gaussian to the fitting function, as shown in the figure. Another fitting function we use is two half Gaussians with identical centroids but independent widths; the amplitudes are coupled to make the function continuous. For the results reported in this paper, we use this second fitting function, even though it gives slightly worse residuals, since it has the advantage of giving more

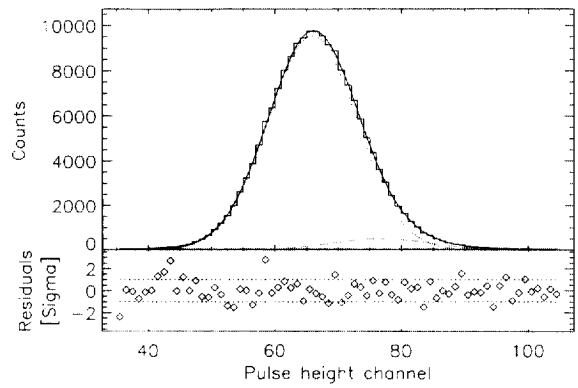

Fig. 3. Fitted spectrum from NaI(Tl) detector with monochromator set to 16 keV. Including a second Gaussian in the fitting function is one way to model the slight asymmetry in the photopeak.

consistent results for the fitted centroid. Depending on which fit is used, the energy-light output relation differs by a maximum of 0.5%, not including an overall gain factor. These systematic uncertainties are folded through our analysis and included in our reported error estimates.

Another systematic effect in our data is that the measured K-escape fractions are lower than expected by up to a factor of two. Our expectations are based on a version of Axel's formula [12] that we modified to take into account the finite thickness of the crystal. Previous measurements of ours have shown the validity of this formula. Measurements of the pulse shape discriminator edges do not give any indication of the cause of this effect. The crystal temperature did not change enough to move any significant portion of the pulse shape distribution outside of the discriminator window. The K-escape peak data are not included in this analysis, and we have no reason to believe that whatever distorted them is having any effect on the photopeak centroid measurements that is larger than the other systematic effects being included in the analysis.

It is necessary in our monochromator data to correct for gain changes in the crystal light output; the changes are believed to be caused by temperature fluctuations. By using overlapping energies during three data runs taken over two days, we could see gain variations of up to 1% between runs. These variations only occur on long time scales since our detector has a high thermal mass. To correct for the observed gain changes in the monochromator data, we applied a separate gain correction factor to each of the three data sets to get the best overlap between them in their light output response to X-rays. Applying these gain factors made the three data sets all consistent with each other.

To be sure that we fully account for temperature effects, we fold different temperature-time profiles into our analysis to determine our sensitivity to this effect. For each sample temperature-time profile, we determine the gain variations to expect, adjust our light output measurements accordingly, and fold these adjusted measurements through our entire analysis. We allow for variations within a given data set of up to $\pm$ 1°C and assume that the mean light output of NaI(Tl) decreases at a rate of $\sim 0.4\%/^{\circ}C$ [13] as temperature is increased. The uncertainties derived from these calculations are included in our results.

2.3. *Radionuclides and fluorescent sources*

The X-ray response measurements are extended to higher energies using laboratory sources. A total of 18 lines from radionuclide and fluorescent sources (Table 1) were used to test each of six flight phoswich detectors. The sources illuminated the full face of each detector at near-normal incidence. Depending on the source, placement was from 24 to 48 inches in front of the detector. A radioactive ^{57}Co source was employed near each detector during these measurements for monitoring overall detector/electronics gain. Since the spectra of most of the lab sources are complicated by such effects as Compton scattering internal to the source itself, a high-resolution germanium detector was used to measure these spectra independently, and results from these measurements were used in fitting the data from the broader-resolution NaI(Tl) crystals.

The electronics setup used with the radionuclide and fluorescent sources was similar to that shown for the monochromator measurements in Fig. 2. One difference is that in the former the LSA time constant was set to 1.5 μs, while in the latter it was set to 500 ns. Apart from an overall normalization

Table 1
Laboratory lines used in response study. For radionuclides, the purchased isotope is shown, and, if the line is a gamma ray, the first decay or transition is also shown [14,15].

Energy (keV)	Photons	Source
14.41	γ-rays	$^{57}Co \xrightarrow{EC} {}^{57}Fe^{*}$
17.44	Mo K_α X-rays	Fluorescence
22.10	Ag K_α X-rays	^{109}Cd
24.14	In K_α X-rays	Fluorescence
26.27	Sb K_α X-rays	Fluorescence
27.38	Te K_α X-rays	^{123m}Te
28.51	I K_α X-rays	Fluorescence
30.85	Cs K_α X-rays	^{133}Ba
34.57	Ce K_α X-rays	Fluorescence
37.19	Nd K_α X-rays	Fluorescence
39.91	Sm K_α X-rays	Fluorescence
42.76	Gd K_α X-rays	Fluorescence
46.52	γ-rays	$^{210}Pb \xrightarrow{\beta} {}^{210}Bi^{*}$
59.54	γ-rays	$^{241}Am \xrightarrow{\alpha} {}^{237}Np^{*}$
80.87	γ-rays	$^{133}Ba \xrightarrow{EC} {}^{133}Cs^{*}$
88.03	γ-rays	$^{109}Cd \xrightarrow{EC} {}^{109m}Ag$
122.06	γ-rays	$^{57}Co \xrightarrow{EC} {}^{57}Fe^{*}$
158.99	γ-rays	$^{123m}Te \xrightarrow{IT} {}^{123}Te^{*}$

factor, we do not expect this difference to affect the shape of the X-ray response curve more than the other uncertainties included in the analysis.

The radionuclide/fluorescent source data is corrected for offset effects (see Section 2.2 and Eq. (1)) by comparison to the monochromator light output response data; the monochromator data is assumed to be perfectly corrected for offset effects since it incorporates the most rigorous testing for this effect. A chi-squared minimization fit is used to determine the best offset correction and gain factor to be applied to each of the six radionuclide/fluorescent source data sets. A substantial improvement is observed in the consistency between the six data sets; the rms variation between the pulse height responses of the six detectors drops from $\pm$ 1.6% (when allowing only for arbitrary gain normalizations) down to $\pm$ 0.3% (when offsets are allowed to vary also).

Although we believe our data to be corrected for all offset effects, we note that the Collinson and Hill procedure is constructed in such a way that any non-zero offset terms cancel out and do not affect the results. As will be discussed, the Collinson and Hill procedure involves taking the difference of two light output measurements. If the corresponding pulse height measurements are each contaminated with the same offset term, then the offset terms will cancel out in the difference.

3. Energy-light output relation for NaI(Tl)

Fig. 4 shows the light output response of the NaI(Tl) crystal plotted as light output divided by X-ray energy vs. X-ray energy. The light output from the crystal is taken as proportional to the centroid obtained from the multiparameter fitting process (see Section 2.2 and Fig. 3). The diamonds represent the measurements taken with the monochromator. Statistical uncertainties for these points are of order the size of the symbol. Systematic uncertainties amount to $\pm$ 0.7%. The squares in the figure reflect the measurements from the radionuclide and fluorescent sources averaged over the six detectors tested in the laboratory. The data are arbitrarily normalized at 88.03 keV, the energy of a line from ^{109}Cd.

Overlaid in Fig. 4 are plots of two functions fit to the data, one above and one below the discontinuity at the iodine K-edge (33.17 keV). The fit above the K-edge is used to create a finely sampled X-ray

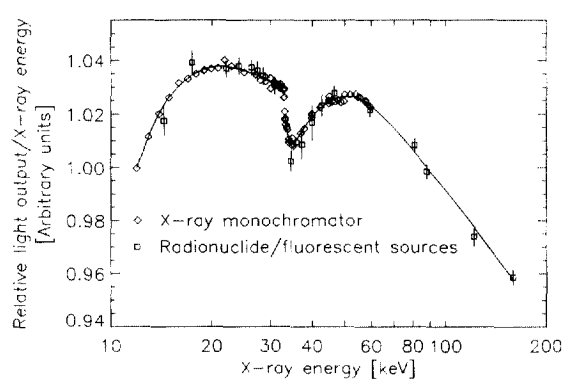

Fig. 4. Light output response of NaI(Tl), normalized at 88.03 keV. Solid line shows a fit to the data. The section of line above the discontinuity at the iodine K-edge is used in the Collinson and Hill procedure.

response curve that is then used in the Collinson and Hill procedure.

4. Response of NaI(Tl) to electrons

4.1. Modified Collinson and Hill procedure

In this section we describe the Collinson and Hill procedure [2] in detail, including several modifications that have been made to the original formulation.

The paradigm that the Collinson and Hill procedure uses is that the response of the NaI(Tl) crystal to X-rays can be recast in terms of the response of the crystal to electrons. An X-ray absorbed by the NaI(Tl) crystal leads to the liberation of a number of electrons. These include photoelectrons and Auger electrons in the models created so far. These electrons then each act independently of each other and lead to the production of light through the scintillation mechanism. A function is used to relate the initial energy of an electron to the mean light yield that it produces. The goal of the Collinson and Hill procedure is to determine this electron response function.

The strategy behind the Collinson and Hill procedure is to take advantage of the fact that when an incident X-ray is photoelectrically absorbed, the excited atom relaxes by a set of processes that are independent of the energy of the absorbed X-ray. Thus, the light output from the crystal is thought of as the sum of two components: (1) the light output due to the initial photoelectron ejected by the incident X-ray, and (2) the light output due to the cascade of electrons liberated during the de-excitation of the atom, including those liberated after various fluorescent photons are reabsorbed in other parts of the crystal. The light output from component (2) will mostly (but not completely – see below) cancel out in the difference, $L_{\gamma} - L_{K^-}$, between mean light yields at the two energies, E_{γ} and E_{K^-}, where E_{γ} is any arbitrary energy above the iodine K-edge, and E_{K^-} is an energy epsilon above the K-edge. Therefore, the Collinson and Hill method has the advantage that, by analyzing differences in light output, the analysis depends less on having a detailed knowledge of the complicated distribution of electrons that are liberated as higher and higher atomic shells in the crystal participate in the cascade process. These complicated processes tend to cancel out. Another advantage of analyzing differences in light output is that, by choosing X-ray energies near the iodine K-edge, we can obtain an accurate map of the response of the crystal to low energy electrons. The K photoelectron that $\sim 83\%$ of the time is ejected by the incident X-ray has energy $E_{\gamma} - E_{K}$, and E_{γ} can be chosen to probe low energy electrons.

We stated that the light output from component (2) does not completely cancel out in the difference $L_{\gamma} - L_{K^-}$. That is because there is an energy dependence to component (2); the K-escape fractions change with energy. Even if this effect is not considered, the Collinson and Hill method is still valid to the degree to which the effect is small and varies slowly with energy. However, we have improved the method by including the K-escape fractions, as described below.

The first step in the Collinson and Hill procedure is to generate a model of the electrons that are liberated within the crystal when an incident X-ray, of energy greater than the iodine K shell binding energy (33.17 keV), loses all of its energy to the crystal. In the electron liberation model that Collinson and Hill originally used, the incident X-ray of energy E_{γ} first interacts in the crystal by being photoelectrically absorbed in either the iodine K or L shell. The probabilities for these two interactions are given by $\sigma_K/(\sigma_L + \sigma_K)$ and $\sigma_L/(\sigma_L + \sigma_K)$, respectively. (The K/L ratio of photoelectric cross sections for the iodine shells is assumed to be independent of energy above the iodine K-edge.) If the interaction is in the K shell, then a photoelectron of energy $E_{\gamma} - E_K$ is liberated. The K shell vacancy leads to the emission of either a characteristic X-ray or an Auger electron, with the fluorescent yield being ω_K. When a vacancy in the K shell leads to fluorescence, i_{α} and i_{β} are the respective probabilities for the emission of a K_{α} and a K_{β} X-ray. The energy of a K_{α} X-ray is taken as $E_K - E_L$, and the energy of a K_{β} X-ray is taken as $E_K - E_M$. If the K_{α} and K_{β} X-rays are absorbed before escaping the crystal, then they are assumed to be absorbed in the iodine L shell, leading to the emission of another photoelectron. For the purpose

of computing the energy of this ejected L shell photoelectron, the binding energy of the L shell is taken as $E_{L'}$; $E_{L'}$ is different from E_L, in that the former is an average of the L subshell energies that is weighted in a manner appropriate for photoelectric cross sections, while the latter is weighted in a manner that is more appropriate for considering Auger and fluorescence transitions that involve the L shell. Vacancies in the iodine L and M shells are assumed to be filled by Auger transitions, and it is approximated that all of the binding energy of the shell with the vacancy goes into the kinetic energy of a single Auger electron. When a vacancy in the iodine K shell leads to an Auger transition, two possibilities are considered; the Auger transition can result in two L shell vacancies, or in one L shell vacancy and one M shell vacancy. The relative probabilities for these two transitions are taken as a_1 and a_2, respectively.

Thus there are several different "cascade sequences" that can occur, by which the energy of a given X-ray is transferred to the kinetic energy of a group of electrons in the crystal. Each sequence results in a certain spectrum of electron energies. Collinson and Hill's original model allowed for five such sequences. Our model, which will be described in the next section, allows for 98 cascade sequences.

In addition to the physical constants listed above, K-escape probabilities are needed to describe the relative probability weightings between the different cascade sequences. Even though we are only considering instances where the full energy of the incident X-ray is absorbed in the crystal, K-escape probabilities are needed to provide, for example, the relative weighting between cascade sequences which do and do not involve an intermediate K X-ray photon. Collinson and Hill did not include K-escape probabilities in their original analysis, and Meggitt [7] noted the correction.

The function $F(E)$ is used to describe the mean scintillation light yield as a function of initial electron energy, E. This function can be folded with the weighted model distribution of electrons that are liberated following the absorption of an X-ray. This determines the mean light yield from the crystal.

We then have the following expression for the mean scintillation light yield collected from the crystal after the full energy of an incident X-ray, $E_\gamma > E_K$, is transferred to the kinetic energy of a group of electrons:

$$
\begin{aligned}
L_\gamma = \frac{1}{G(E_\gamma)}\Bigg[& \frac{\sigma_K}{\sigma_L+\sigma_K}\{(1-P_{K_\alpha}(E_\gamma))\omega_K i_\alpha \\
& \times [F(E_\gamma - E_K) + F(E_K - E_{L'} - E_L) \\
& + F(E_{L'}) + F(E_L)] \\
& + (1-P_{K_\beta}(E_\gamma))\omega_K i_\beta [F(E_\gamma - E_K) \\
& + F(E_K - E_{L'} - E_M) + F(E_{L'}) + F(E_M)] \\
& + (1-\omega_K)a_1[F(E_\gamma - E_K) + F(E_K - 2E_L) \\
& + 2F(E_L)] + (1-\omega_K)a_2[F(E_\gamma - E_K) \\
& + F(E_K - E_L - E_M) + F(E_L) + F(E_M)]\} \\
& + \frac{\sigma_L}{\sigma_L+\sigma_K}\{F(E_\gamma - E_{L'}) + F(E_{L'})\}\Bigg],
\end{aligned}
\tag{2}
$$

$$
\begin{aligned}
G(E_\gamma) = \frac{\sigma_K}{\sigma_L+\sigma_K}\{ & (1-P_{K_\alpha}(E_\gamma))\omega_K i_\alpha \\
& + (1-P_{K_\beta}(E_\gamma))\omega_K i_\beta \\
& + (1-\omega_K)(a_1+a_2)\} + \frac{\sigma_L}{\sigma_L+\sigma_K}.
\end{aligned}
$$

$P_{K_\alpha}(E_\gamma)$ and $P_{K_\beta}(E_\gamma)$ are the probabilities that a K_α or K_β X-ray will escape the crystal, given that the incident X-ray is photoelectrically absorbed in the iodine K shell, that the iodine atom relaxes by fluorescence, and given whether a K_α or K_β X-ray is produced by the fluorescence. Eq. (2) is the equivalent of what Collinson and Hill labelled Eq. (1) in their original analysis, except modified as Meggitt did to account for K-escape probabilities.

The next step in the Collinson and Hill procedure is to write down an expression for $L_\gamma - L_{K'}$, using Eq. (2). This expression is rearranged to solve for $F(E_\gamma - E_K)$, as a function of $L_\gamma - L_{K'}$, and of the electron response, F, at a number of discrete energies.

An initial estimate must be made of the electron response curve, in order to seed the Collinson and Hill procedure, which is an iterative procedure. We use the same initial estimate as Collinson and Hill: $F(E_\gamma - E_K) \approx L_\gamma - L_{K'}$. Thus, by using the fit to

the X-ray response data shown in Fig. 4, we obtain an initial estimate for $F(E)$. We tried several other initial estimates for $F(E)$ and found that the procedure converged to the same result for each one.

The final step in the procedure is to perform the iterations. With each iteration, the new electron response curve is computed using the equation for $F(E_\gamma - E_K)$; the electron response function, $F(E)$, from the previous iteration and the measured values of $L_\gamma - L_K$ are substituted into the equation. The iterations are performed until the response curve stops changing by more than 0.1% between iterations.

In their original analysis, Collinson and Hill included one more step, which we believe is better to omit. They adjusted their electron response curve to make the X-ray light output predicted by Eq. (2) match the experimental X-ray data. This has the undesireable effect of making the results more dependent on the differences that exist between the true atomic physics and our model approximation of these processes; it destroys the inherent strength that the Collinson and Hill method has of being able to cancel out these differences.

4.2. Expanded model of atomic processes

In this section we describe how we expand on the model Collinson and Hill originally used, to include a much more detailed description of the cascade liberation of electrons that follows the absorption of an incident X-ray.

For modelling photoelectric interactions, the atom is represented by the iodine K shell, the iodine L shell divided into its three subshells, the iodine M_I shell, and the sodium K shell. The shells higher than these are collapsed into a single equivalent shell, whose photoelectric cross section is taken as the sum of the photoelectric cross sections for all these higher shells, and whose binding energy is taken as the average of that for the iodine M_{II-V} shells.

Both fluorescence and Auger transitions are tracked in the iodine K and L shells. All other shells are assumed to undergo an Auger transition if excited.

For Auger transitions that are triggered by a vacancy in a shell other than the iodine K shell, it is approximated that the atom relaxes in a single step with the liberation of a single electron whose kinetic energy is equal to the binding energy of original shell. Auger transitions triggered by a vacancy in the iodine K shell are broken down into three classes – those ending with two holes in the iodine L shell, those ending with one hole in the iodine L shell and one hole in a higher iodine shell, and those ending with two holes in higher iodine shells. When modelling the Auger transitions, the L shell binding energy is taken as an average of the three L subshell binding energies, and the binding energy of the "higher" shell is taken as the average of the binding energies for the iodine M_{I-V} shells.

Characteristic K X-rays produced by iodine atoms are broken down into K_{α_1}, K_{α_2}, and K_β X-rays.

The values of physical constants are obtained from several sources. Photoelectric cross sections are obtained from Berger and Hubbell [16]. Data from Storm and Israel [17] are used for the fluorescent yields, the binding energies of the atomic shells, and the relative intensities of emission for the different X-rays. The relative probabilities of the different K shell Auger transitions are taken from Wapstra et al. [18].

Our model contains a total of ninety-eight cascade sequences by which an X-ray of energy greater than the K shell binding energy can transfer its energy to the electrons. Each of the ninety-eight cascade sequences results in the liberation of two to eight electrons, depending on the physics involved. Fig. 5 shows a histogram of the weighted distribution of energies of all liberated electrons, from all ninety-eight cascade sequences, for the case of a 45 keV X-ray incident on the crystal. The bins are each 1/3 keV wide. The histogram is arbitrarily normalized to 100.0 for the spike at 12 keV, which corresponds to a K photoelectron ejected by the incident 45 keV X-ray.

The effects of scattering (Compton and Rayleigh) are not included in our derivation of the electron response curve. As Compton interactions involve the liberation of a recoil electron into the crystal, these recoil electrons can affect the calculation of the electron response. The effect is not expected to be large, however, since the number of Compton interactions during full energy loss events is kept

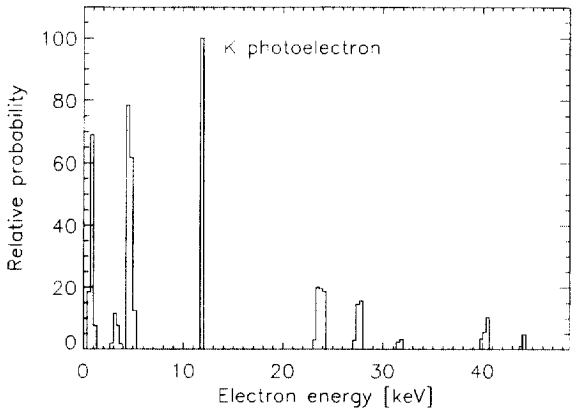

Fig. 5. Model distribution of energies of Auger electrons and photoelectrons liberated in NaI(Tl) following the absorption of a 45 keV X-ray. Electron energies are histogrammed together in 1/3 keV bins.

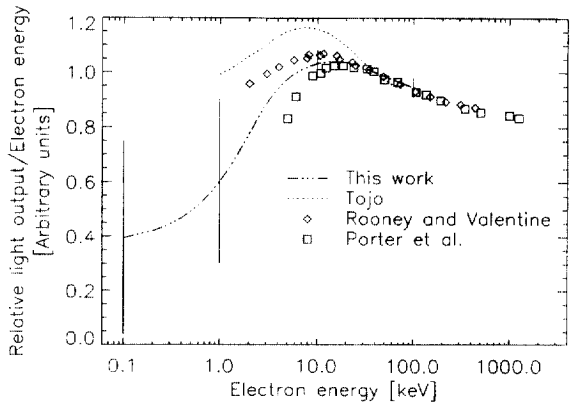

Fig. 6. Light output response of NaI(Tl) crystal to 0.1–125 keV electrons. All curves normalized at 40 keV. Dashed line: this work; closed circles: Tojo [3]; diamonds: Rooney and Valentine [6]; squares: Porter et al. [10].

low by the thin dimensions of our crystal, and since the Compton cross section is at least an order of magnitude lower than the photoelectric cross section over almost the entire energy range of interest. To quantify this effect, we ran a Monte Carlo routine, specific to our crystal geometry, that included tracking of Compton interactions. We considered only those events where the full energy of the incident photon was lost to the NaI(Tl) crystal. The Monte Carlo results allowed us to see the number of events in which Compton interactions were involved, which photons (e.g., incident or intermediate K X-ray) underwent a Compton interaction, and the distribution of Compton recoil electron energies. Using this information, we estimated the errors in our final electron response curve caused by Compton interactions and included these estimates in our reported uncertainties. We also considered Rayleigh scattering in the crystal. Even though the Rayleigh cross section dominates the Compton cross section in NaI(Tl) below ~ 85 keV, Rayleigh interactions are not important to this analysis since these scatterings are elastic and no electrons are liberated in the process. The Rayleigh scatterings will have a small effect on things such as the K-escape fraction, but we believe such effects are within the uncertainties already quoted.

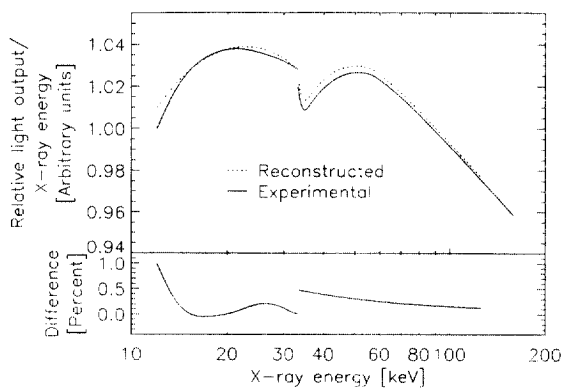

Fig. 7. Top panel shows a comparison of the experimental data (normalized to 1.0 at 88.03 keV) versus the reconstructed model prediction. Bottom panel shows the residuals.

4.3. Electron response curve

The final electron response curve is shown in Fig. 6. The one-sigma uncertainties in our results are estimated at $\pm 90\%$ at 0.1 keV, $\pm 50\%$ at 1 keV, $\pm 5\%$ at 10 keV and $\pm 4\%$ at 100 keV.

The electron response curve and the model of electron energy distributions are used to reconstruct the X-ray light output response curve, as a check on our results. We compare the reconstructed curve to the experimental curve in Fig. 7. No free normalization parameters are used to align the

two curves. The comparison is extended to energies below the iodine K-edge, using the same electron response curve and a model of electron energy distributions appropriate for this lower energy region. The data and the model agree well with residuals of less than 1% at all energies. Contributions to the residuals can include any of the differences that exist between the true atomic physics of the detector and our model of atomic processes – e.g., uncertainties in how to model the higher atomic shells, the role of Compton scattering, any energy dependence to the ratios of photoelectric cross sections in different shells, etc.

4.4. Surface effects

One of the primary goals of our analysis is to obtain a clearer understanding of the intrinsic physical processes that occur during the scintillation response of NaI(Tl). Towards this end, we want to avoid using data taken where the intrinsic nature of the NaI(Tl) scintillation mechanism is unduly distorted by surface effects (e.g., contaminants or crystal defects). Concern was raised by Meggitt [7] that previous analyses similar to ours may be affected in this way. In this section we describe a search of our data for surface effects and conclude that there is no evidence that such effects are distorting our data.

Surface effects have been shown to be capable of playing a role in the scintillation response of NaI(Tl) to X-rays. Kaiser et al. [5] showed that the measured energy-light output relation of NaI(Tl) is sensitive to surface treatment at low input photon energies ($\lesssim$20 keV). Narayan and Prescott [19] showed that the measured discontinuity in pulse height resolution at the iodine K-edge is also sensitive to surface preparation. Despite these phenomenological results, not much is known about the physics of how surface conditions distort the data.

Meggitt [7] developed a model of surface conditions and their effect on the response of NaI(Tl). We apply this model to our data to make an estimate of the degree to which surface effects might distort our results. Meggitt modelled the NaI(Tl) crystal as having a reduced scintillation efficiency near the surface. The light output, $L(x)$, from electrons liberated between distances x and $x + dx$ from the surface is taken as

$$L(x)/L_0 = 1 - e^{-\lambda x}, \tag{3}$$

where L_0 is the light output from the same electron in the bulk of the crystal, and λ parameterizes the surface layer. The liberated electrons are assumed to lose all of their energy to the crystal within a range that is very small compared to the 1/e thickness of the surface layer.

Meggitt's approach to estimating λ was to look at the magnitude of the measured discontinuity in relative variance, $V_s = \sigma^2_{\rm rms}/\overline{L}^2$, upon crossing the iodine K-edge. As Meggitt noted, a surface layer described by Eq. (3) makes its own contribution to the detector resolution; the light output due to an absorbed photon varies depending on the depth below the surface at which the photon is absorbed, and depending on the depth at which any subsequent characteristic X-rays are absorbed. Additionally, as Meggitt noted, this contribution to the detector resolution is discontinuous across the iodine K-edge, because an increase in photoelectric cross section causes photon interactions to occur closer to the surface. Meggitt assumed that the measured discontinuity in resolution was due solely to the surface layer described by Eq. (3). Meggitt developed a relation to describe λ as a function of the magnitude of this discontinuity.

We disagree with several points in Meggitt's analysis.

1. In Eq. (6) of Meggitt, the weighting factor $e^{-\mu x}$ is used to describe the distribution of depths within the crystal at which incident X-rays that contribute to the photopeak are photoelectrically absorbed. However, this weighting factor is not correct for cascade sequences (or "interaction types" as Meggitt denotes them) that involve an intermediate K fluorescent photon. These K photons are more likely to escape the crystal when they are generated near the surface; if a K photon escapes, then that event will not be included in the photopeak. This causes the distribution of absorption depths within the crystal to no longer be a simple exponential.

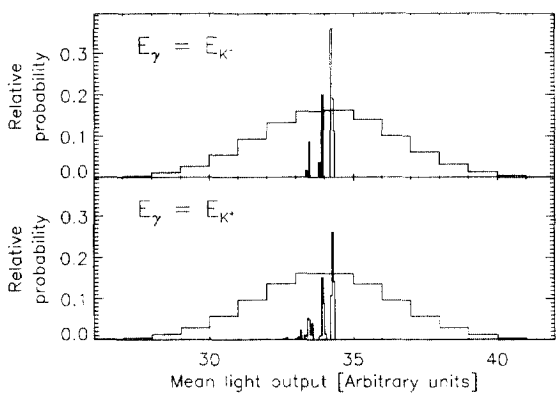

Fig. 8. Histogrammed distribution of mean light output values from the different cascade sequences. The measured electron response curve was folded through our electron liberation model. The two panels correspond to input energies that are epsilon above and below the iodine K-edge. Superimposed on each is a graph of what the photopeak looks like after other sources of resolution broadening are included.

2. Eq. (9) of Meggitt assumes that the variances due to different cascade sequences can be added together, as if combining the output from different cascade sequences is the same as summing independent random variables. However, the outputs from the different cascade sequences cannot be combined in this way. A Monte Carlo routine, written with Meggitt's set of initial assumptions, yields significant differences compared to what the equations predict. For example, for the case of an input photon of energy 35 keV, a $\lambda = 200\,\mathrm{cm}^{-1}$ surface layer parameter, and with Meggitt's n value set to 0.2, the Monte Carlo routine and Meggitt's equations differ by $\sim 60\%$ for the value of the relative variance, $V_s = \sigma^2_{\mathrm{rms}}/\bar{L}^2$.
3. There are several other effects besides surface effects that contribute to the discontinuity in resolution at the iodine K-edge, and it may or may not be fair to approximate surface effects as the dominant contribution to the discontinuity. One example of another contribution to the discontinuity in resolution is illustrated in Fig. 8. The distribution of mean light output values from the different cascade sequences changes discontinuously on crossing the K-edge. (Note that details in the appearance of Fig. 8 are sensitive to the model chosen to describe the different cascade sequences, and that the figure may change noticeably as the model is further improved; we include the figure anyway because it serves to illustrate the results of our modelling, because it provides an interesting picture of the scintillation response of NaI(Tl), and because it helps illustrate our point about the discontinuity in resolution at the iodine K-edge.)

We decided to use a different method to estimate a lower limit to λ (i.e., an upper limit to the 1/e thickness of the surface layer). A surface layer with an appreciable thickness to it will significantly distort the symmetry of a photopeak produced by monoenergetic X-rays. The low side of the photopeak will develop a tail extending to low pulse height values. The relatively symmetrical shape of the photopeaks from our monochromator data then allows us to place a lower limit on the value of λ for these data. We wrote a Monte Carlo routine to estimate the change in the shape of the photopeak as a function of λ. The routine tracks a large number of monoenergetic photons normally incident on the face of the crystal. The Monte Carlo routine uses Eq. (3) to determine the relative amount of scintillation light each photon produces. This is done by recording the depth below the surface at which the incident photon is absorbed and the depth below the surface at which any subsequent K or L characteristic X-rays are absorbed. If any K and/or L X-rays escape the crystal, then the portion of the light output due to those characteristic X-rays is taken as zero. It is assumed that the electron scintillation response is proportional to electron energy for this investigation. Scattering effects are neglected in the Monte Carlo routine since the scattering cross section is such a small fraction of the photoelectric cross section at low energies (4% at 16 keV).

The results from a Monte Carlo run using Meggitt's value of $\lambda = 200\,\mathrm{cm}^{-1}$, which corresponds to a 1/e thickness of 50 μm, for the case of 16 keV photons incident on the crystal, are shown in Fig. 9. The scintillation light output responses from all the Monte Carlo events are binned together, and the histogram is plotted in the top panel. This

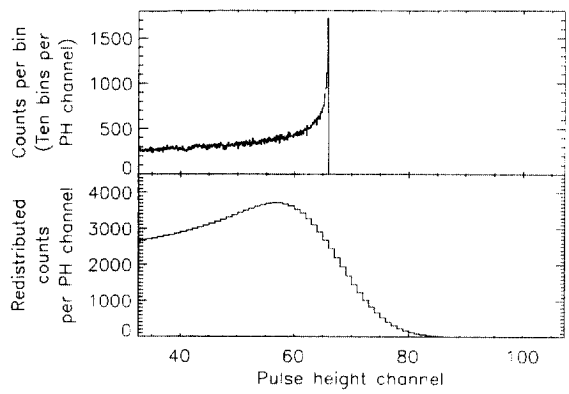

Fig. 9. Top plot shows results, from a Monte Carlo simulation, of how a surface layer of reduced scintillation efficiency with $1/e$ thickness of 50 μm would distort the unbroadened light output response to a 16 keV monochromatic beam. Bottom plot shows the same data after applying resolution broadening. Significant distortion of the photopeak is seen.

histogram represents what the 16 keV photopeak would look like if there were no resolution broadening due to anything except surface effects. The tail that extends to low pulse heights is due to photoelectric interactions that occur near the surface of the crystal resulting in reduced scintillation light output. If there were no surface layer effect, then the histogram would just be a delta function. To estimate what the final pulse height spectrum would look like if such a surface layer were present, we apply resolution broadening individually to each of the bins in the top panel of Fig. 9 and then sum them all together to get the result shown in the bottom panel of the figure. We use broadening parameters that would give a spectrum identical to the peak in Fig. 3 if the top panel in Fig. 9 had been a delta function. The bottom panel of Fig. 9 can be compared directly to the photopeak in Fig. 3. Clearly our data do not indicate an effect of this magnitude.

From the symmetry of the photopeaks in our data, we can put an upper limit on the $1/e$ thickness of the surface effect of 1.4 μm, or $\lambda = 7 \times 10^3\,\mathrm{cm}^{-1}$.

This value for the $1/e$ thickness is so small that it may no longer be valid to assume that the liberated electrons all lose their energy in a distance which is small compared to the $1/e$ thickness of the surface layer. To improve the model, one would have to better account for the path of the liberated electrons. Employing this level of detail to study surface effects is beyond the scope of our analysis.

Though this assumption about the electron paths may not hold, we still want to know if the model suggests that our data may be distorted by surface effects. We use the model to make an estimate of how a $\lambda = 7 \times 10^3\,\mathrm{cm}^{-1}$ surface layer would distort our results. We take a distribution like the one from the bottom of Fig. 9, but equivalent for a $\lambda = 7 \times 10^3\,\mathrm{cm}^{-1}$ surface parameter, and fit it with a Gaussian curve. Immediately above the K-edge, a $\lambda = 7 \times 10^3\,\mathrm{cm}^{-1}$ surface effect causes the light output centroid to decrease by only 0.2%. This is within the uncertainties already quoted for our light output measurements.

We thus summarize surface effects as follows. Applying the model described by Eq. (3) does not give any indication that surface effects are important to our analysis, though one assumption that goes into the model may not be entirely valid. We cannot rule out surface effects as an issue. Indeed there is experimental evidence that surface conditions can affect the light output response of NaI(Tl). 22% of X-rays of energy just above the iodine K-edge are absorbed within 20 μm of the surface. It is not inconceivable that there are surface effects that follow some other model.

5. Comparison to other electron response measurements

Fig. 6 compares measurements of the response of NaI(Tl) to electrons, performed using various techniques. Rooney and Valentine [6] measured the response of NaI(Tl) to individual Compton recoil electrons. Porter et al. [10] bombarded NaI(Tl) directly with electrons and reported that, at low energies (< 10 keV), surface effects on the crystal might be distorting the results. Tojo [3] also applied the Collinson and Hill procedure to X-ray data, though the correction for K-escapes that Meggitt noted was apparently not included in the analysis. A number of other authors have also used X-ray response data to infer the response of NaI(Tl)

to electrons, but in Fig. 6 we have only included results from the two reports (Tojo's and ours) that use the most detailed models for the spectrum of liberated electrons.

Since the electron response curve only describes relative light output and not absolute light output, comparisons between measurements from different groups must be done after normalizing the response curves. All the methods just described for determining the electron response have their smallest systematic errors in the region of higher electron energies. Thus, all the results in Fig. 6 were normalized at an energy of 40 keV. The resulting spread is $\pm$ 4% or less above 20 keV, and increases at lower energies.

Our results agree, within uncertainties, with Porter and with Rooney and Valentine. Our results are not consistent with Tojo.

The data of Rooney and Valentine offer the electron response measurement with the smallest uncertainties at low energies. Their reported uncertainties are no larger than $\pm$ 2% anywhere on the response curve. Our results cannot reach this level of precision, despite the high quality of our data and all the improvements we include to the analysis. The uncertainties in our results arise from a number of effects that are inherent to the Collinson and Hill procedure, but to which the Rooney and Valentine technique is immune – e.g., small differences in the measured X-ray response can have a significant impact on the inferred electron response.

Also, unlike the results of Rooney and Valentine, our results could be distorted by surface effects, even though we did not find any evidence for these effects in a search of our data.

There is one other way in which the Rooney and Valentine technique is more robust than the Collinson and Hill procedure. In the Collinson and Hill procedure, we assume that the liberated electrons each act independently in the scintillation process. Even though a number of the liberated electrons may follow tracks that are near to each other in the crystal, the scintillation process due to one electron is assumed not to interfere with the scintillation process of another electron. If any interference does exist, then the light output due to an absorbed X-ray would be more complicated to determine. In this regard, Rooney and Valentine's Compton Coincidence Technique may have an intrinsic advantage over the Collinson and Hill procedure; by exciting the crystal with essentially just one electron at a time, there is less of a question about electron independence.

Our measurements do have the advantage of extending to lower energies than other authors report. Rooney and Valentine's technique is difficult to extend down to 0.1 keV. The Collinson and Hill technique allows for these low energy measurements. However, previous authors who have used the Collinson and Hill technique, or related procedures, have not extended down to these low energies because they have not had X-ray data on such a fine energy grid around the iodine K-edge.

6. Conclusion

We have measured the response of NaI(Tl) to X-rays in the energy range 12–159 keV, with special emphasis near the K-edge of iodine. From these data, we have inferred the response of NaI(Tl) to electrons in the energy range 0.1–125 keV. This was done using a modified version of the Collinson and Hill procedure, that includes a more detailed model of the cascade liberation of electrons, has a full treatment of K-escape effects, and omits a step from the original procedure that would hurt the results more than it would help. We have included a careful consideration of surface effects. The electron response has been measured down to an energy lower than has been previously examined. The electron response is determined to a precision of $\pm$ 90% at 0.1 keV, $\pm$ 50% at 1 keV, $\pm$ 5% at 10 keV and $\pm$ 4% at 100 keV.

An improvement to the Collinson and Hill procedure would be as follows. Whereas currently the procedure involves a set of equations, the use, instead, of a Monte Carlo program might represent an improvement. One advantage would be the elimination of equations that are becoming very large. Additionally, such a change would, for the first time, allow one to directly account for scattering processes while using the Collinson and Hill procedure.

Acknowledgements

Thanks to Gregory Wood for assisting with the energy calibration of the monochromator, to George Huszar and Phil Blanco for assisting with the Monte Carlo simulation, and to David Band, Duane Gruber, Richard Lingenfelter, Jim Matteson, and Mike Pelling for helpful discussions. Also thanks to Peter Siddons, Jerry Hastings, and the staff of Brookhaven's National Synchrotron Light Source for allowing us time on the development beamline and their support of our efforts. This research was supported by NASA contract NAS5-30720.

References

[1] D.E. Gruber, P.R. Blanco, W.A. Heindl, M.R. Pelling, R.E. Rothschild, P.L. Hink, Astron. Astrophys. Suppl. Ser. 120 (1996) 641.
[2] A.J.L. Collinson, R. Hill, Proc. Phys. Soc. 81 (1963) 883.
[3] T. Tojo, Nucl. Instr. and Meth. A 241 (1985) 177.
[4] T.H. Jones, Nucl. Instr. and Meth. 15 (1962) 55.
[5] W.C. Kaiser, S.I. Baker, A.J. MacKay, I.S. Sherman, IEEE Trans. Nucl. Sci. 9 (1962) 22.
[6] B.D. Rooney, J.D. Valentine, IEEE Trans. Nucl. Sci. 43 (1996) 1271.
[7] G.C. Meggitt, Nucl. Instr. and Meth. 83 (1970) 313.
[8] C.D. Zerby, A. Meyer, R.B. Murray, Nucl. Instr. and Meth. 12 (1961) 115.
[9] R. Hill, A.J.L. Collinson, Brit. J. Appl. Phys. 17 (1966) 1377.
[10] F.T. Porter, M.S. Freedman, F. Wagner Jr., I.S. Sherman, Nucl. Instr. and Meth. 39 (1966) 35.
[11] M.F. McCann, K.M. Smith, Nucl. Instr. and Meth. 65 (1968) 173.
[12] P. Axel, Rev. Sci. Instrum. 25 (1954) 391.
[13] S.S. Al-Dargazelli, K.H. Al-Attiah, Appl. Radiat. Isot. 40 (1989) 729.
[14] E. Browne, R.B. Firestone, in: V.S. Shirley (Ed.), Table of Radioactive Isotopes, Wiley, New York, 1986.
[15] R.B. Firestone, in: V.S. Shirley (Ed.), Table of Isotopes, 8th ed., Wiley, New York, 1996.
[16] M.J. Berger, J.H. Hubbell, Report NISTIR 87-3597 National Institute for Standards and Technology, 1987 (obtained online from the National Nuclear Data Center, Brookhaven National Laboratory).
[17] E. Storm, H.I. Israel, Los Alamos Scientific Laboratory Report LA-3753, 1967.
[18] A.H. Wapstra, G.J. Nijgh, R. Van Lieshout, Nuclear Spectroscopy Tables, North-Holland, Amsterdam, 1959.
[19] G.H. Narayan, J.R. Prescott, IEEE Trans. Nucl. Sci. 13 (1966) 132.